

NUMERICAL STUDY OF VARIABLE VISCOSITY AND THERMAL CONDUCTIVITY ON MHD NATURAL CONVECTION FLOW ALONG A VERTICAL FLAT PLATE WITH STRESS WORK

Sree Pradip Kumer Sarker¹, Md.M.Alam²

¹M.Phil.Researcher, Dhaka University of Engineering & Technology, Gazipur.

²Professor, Department of Mathematics, Dhaka University of Engineering & Technology, Gazipur.

ABSTRACT: *From a technical standpoint, free convection flow around an isothermal vertical flat plate in the presence of a magnetic field is very critical, and many researchers have studied such problems. The effects of variable viscosity and thermal conductivity on magneto hydrodynamics (MHD) natural convection flow over a heated vertical plate immersed in a fluid with stress work will be investigated in this research. The basic governing equations are converted into non-dimensional governing equations by using the necessary variables. These equations' numerical calculations are carried out using an effective implicit finite-difference system. The Crank-Nicolson scheme is what it's called. This research uses a viscous incompressible fluid with temperature-dependent viscosity and thermal conductivity. The two-dimensional laminar and unsteady boundary layer equations are discussed here. The effect of various parameters on velocity, temperature, local skin friction, local Nusselt number, average skin friction, and average Nusselt number profiles will be seen in this analysis, and the results will be compared to those of other researchers. We'll also make a comparison between the current work's figures and those from previous publications.*

KEYWORDS: Steady State, Magneto-Hydrodynamics, Variable Viscosity, Dependent Thermal Conductivity

INTRODUCTION

The viscous dissipation effect is significant in natural convection in a variety of devices that are subjected to large decelerations or run at high rotational speeds, as well as in strong gravitational field processes on large scales (on large planets) and geological processes. The effects of variable viscosity and thermal conductivity on MHD natural convection flow along an isothermal vertical flat plate with stress work are usually overlooked in discussions and analyses of natural convection flows, friction, and viscous stress work effects. Furthermore, scientists and researchers are interested in the issue of natural convection flow along a vertical flat plate because of its numerous applications. Convection is widely visualized in engineering

applications such as the formation of microstructures during the cooling of molten metals and fluid flows around veiled heat dissipation fins, solar ponds, petroleum reservoirs, nuclear energy, and fire engineering, to name a few. Because of its various applications in the areas of energy conservation, cooling of electrical and electronic devices, construction of solar collectors, heat exchangers, and many others, natural convection heat transfer has gotten a lot of attention. The most difficult aspect of solving natural convection problems is determining the velocity field, which has a significant impact on the heat transfer process. The effect of pressure stress work and viscous dissipation in natural convection flow along a vertical flat plate with heat conduction was studied by Alam et al. [1]. The Joule heating effect on the coupling of conduction with MHD free convection flow from a vertical flat plate was presented by Alim et al. [2]. The effects of temperature-dependent thermal conductivity on MHD free convection flow along a vertical flat plate with heat conduction were investigated by Rahman et al. [3]. Alim et al. [4] investigated the influence of viscous dissipation and Joule heating on conduction and free convection coupling along a vertical flat plate. Molla et al. [5] studied natural convection laminar flow along a vertical wavy surface with temperature-dependent viscosity and thermal conductivity. The effects of temperature-dependent thermal conductivity on natural convection flow along a vertical flat plate with heat generation were presented by Safiqul Islam et al. [6]. The effects of viscous dissipation on MHD natural convection flow along a vertical wavy surface were investigated by Kabir et al. [7]. Hossain [8] investigates the effects of viscous and Joule heating on MHD free convection flow with variable plate temperature. Soundalgekar et al. [9] investigate the finite difference study of transient free convection on an isothermal flat plate. Elbashbeshy et al. [10] investigate a steady free convection flow with variable viscosity and thermal diffusivity along a vertical plate. Kafoussius et al. [12] consider the numerical analysis of the combined free and forced convective laminar boundary layer flow past a vertical isothermal flat plate with temperature dependent viscosity. Anwar Hossain et al. [13] present the effect of radiation on free convection flow of fluid with variable viscosity from a porous vertical plate. Seddeek [14] investigates the effect of variable viscosity on an MHD free convection flow past a semi-infinite flat plate with an aligned magnetic

field in the case of unsteady flow. G.palani.Kwang et al. [18] investigated a numerical analysis of a vertical plate with varying viscosity and thermal conductivity. In this research, an analytical solution for the variable viscosity and dependent thermal conductivity in natural convection flow along a vertical flat plate in the presence of magneto-hydrodynamics with heat conduction will be performed based on experimental analysis. The discretization of momentum and energy equations in terms of non-dimensional coordinates x and y in order to express the equations in finite difference form by approximating functions and derivatives in terms of the core differences in both coordinate directions. The numerical calculations of these equations led to the creation of a programming code for the current problem, which uses an effective implicit finite-difference scheme known as the Crank-Nicolson scheme. For various parameters such as variable viscosity λ , dependent thermal conductivity Y , magnetic parameter M , pressure work parameters Ge , and Prandtl's number Pr , the outcomes data analysis has established for velocity profile, temperature profile, local skin friction local Nusselt number, average skin friction, and average Nusselt number.

MATHEMATICAL ANALYSIS

The unsteady flow of a viscous incompressible fluid past a semi-infinite vertical plate is considered here. As shown in Fig.1, the x -axis is taken vertically upward along the plate, and the y -axis is chosen perpendicular to the plate at the leading edge. The x -axis is assumed to begin at the plate's leading edge. Except for the fluid viscosity, which varies exponentially with fluid temperature, the thermal conductivity, which varies linearly with fluid temperature, and the density variation in the body force term in the momentum equation, where the Bossiness approximation is used, all fluid physical properties are assumed to be constant. The mathematical statement of the basic conservation laws of mass, momentum and energy for the steady viscous incompressible and electrically conducting flow, after simplifying we have

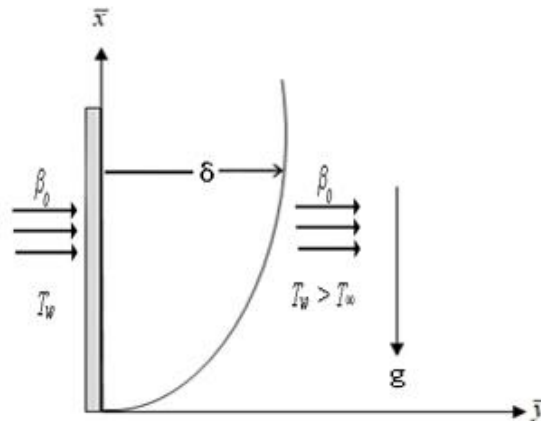


Figure 1

The mathematical statement of the basic conservation laws of mass, momentum and energy for the steady viscous incompressible and electrically conducting flow, after simplifying we have

$$\frac{\partial \bar{u}}{\partial \bar{x}} + \frac{\partial \bar{v}}{\partial \bar{y}} = 0 \tag{1}$$

$$\frac{\partial \bar{u}}{\partial t'} + \bar{u} \frac{\partial \bar{u}}{\partial \bar{x}} + \bar{v} \frac{\partial \bar{u}}{\partial \bar{y}} = \frac{1}{\rho} \frac{\partial}{\partial \bar{y}} \left(\mu \frac{\partial \bar{u}}{\partial \bar{y}} \right) + g \beta (T' - T'_{\infty}) - \sigma_0 \frac{\beta_0^2 \bar{u}}{\rho} \tag{2}$$

$$\frac{\partial T'}{\partial t'} + \bar{u} \frac{\partial T'}{\partial \bar{x}} + \bar{v} \frac{\partial T'}{\partial \bar{y}} = \frac{1}{\rho C_p} \frac{\partial}{\partial \bar{y}} \left(k \frac{\partial T'}{\partial \bar{y}} \right) + \frac{T' \beta \bar{u}}{\rho C_p} \frac{\partial P}{\partial \bar{x}} \tag{3}$$

Where, \bar{u} and \bar{v} are the velocity components along the \bar{x} and \bar{y} axis respectively, t' is the time, T' is the temperature of the fluid in the boundary layer and T'_{∞} is the fluid temperature far away from the plate, g is the acceleration due to gravity, κ is the thermal conductivity of the fluid, ρ is the density, C_p is the specific heat at constant pressure and μ is the variable dynamic co-efficient of viscosity of the fluid. The

hydrostatic pressure $\frac{\partial P}{\partial \bar{x}} = -\rho_e g$ where, $\rho_e = \rho$, $k(T)$ is the thermal conductivity of the fluid depending on the fluid temperature T' , σ_0 is the electric conduction and β_0 is the magnetic field strength.

The initial and boundary conditions are

$$\begin{aligned} t' \leq 0: \bar{u} = 0, \bar{v} = 0, \quad T' = T'_\infty \text{ for all } y, \quad t' > 0: \bar{u} = 0, \bar{v} = 0, \quad T' = T'_w \text{ at } y = 0 \\ t' > 0: \bar{u} = 0, T' = T'_\infty \text{ at } x = 0, \quad t' > 0: \bar{u} \rightarrow 0, \quad T' \rightarrow T'_\infty \text{ as } y \rightarrow \infty \end{aligned} \quad (4)$$

TRANSFORMATION OF THE GOVERNING EQUATIONS

Heat on introducing the following non-dimensional quantities in equations (1) to (4), we have

$$\begin{aligned} x = \frac{\bar{x}}{L}, \quad y = \frac{\bar{y}}{L} Gr^{1/4}, \quad u = \frac{L\bar{u}}{\nu} Gr^{-1/2}, \quad v = \frac{\bar{v}L}{\nu} Gr^{-1/4}, \quad t = \frac{\nu t'}{L^2} Gr^{1/2}, \\ T = \frac{T' - T'_\infty}{T'_w - T'_\infty}, \quad Gr = \frac{g\beta L^3 (T'_w - T'_\infty)}{\nu^2}, \quad Pr = \frac{\mu_0 C_p}{k_0}, \quad \nu = \frac{\mu_0}{\rho} \end{aligned} \quad (5)$$

Here L is the length of the plate, ν is the kinematic viscosity, Gr is the Grashof number, Pr is the Prandtl's number.

Out of many forms of variation of viscosity and thermal conductivity with dimensionless temperature T , which are available in the literature. The following forms are proposed by Statter[21], Ockendon and Ockendon[8], Elbashbeshy and Ibrahi[10], Wilson and Duffy[16], and Seddeek and Abdelmeguid[19]

$$\frac{\mu}{\mu_0} = e^{-\lambda T} \quad (6)$$

$$\frac{k}{k_0} = 1 + \gamma T \quad (7)$$

Where λ and γ denote the viscosity and thermal conductivity variation parameters respectively, depended on the nature of the fluid. Here μ_0 and k_0 are the viscosity and the thermal conductivity at temperature T'_w .

The magneto-hydrodynamic field in the fluid is governed by the boundary layer equations, which in the non-dimensional form obtained by introducing the dimensionless variables described in (5), may be written the equation of continuity as

$$\Rightarrow \frac{\partial\left(\frac{v}{L}Gr^{\frac{1}{2}}u\right)}{\partial(xL)} + \frac{\partial\left(\frac{v}{L}Gr^{\frac{1}{4}}v\right)}{\partial\left(\frac{yL}{Gr^{\frac{1}{4}}}\right)} = 0$$

$$\therefore \frac{\partial u}{\partial x} + \frac{\partial v}{\partial y} = 0 \tag{8}$$

Now momentum equation (2) can be reduced by applying the non- dimensional transformation (5) and (6), we have

$$\Rightarrow \frac{\partial\left(\frac{v}{L}Gr^{\frac{1}{2}}u\right)}{\partial\left(\frac{tL^2}{vGr^{\frac{1}{2}}}\right)} + \frac{v}{L}Gr^{\frac{1}{2}}u \frac{\partial\left(\frac{v}{L}Gr^{\frac{1}{2}}u\right)}{\partial(xL)} + \frac{v}{L}Gr^{\frac{1}{4}}v \frac{\partial\left(\frac{v}{L}Gr^{\frac{1}{2}}u\right)}{\partial\left(\frac{yL}{Gr^{\frac{1}{4}}}\right)}$$

$$= \frac{1}{\rho} \frac{\partial}{\partial\left(\frac{yL}{Gr^{\frac{1}{4}}}\right)} \left(\mu_0 e^{-\lambda t} \frac{\partial}{\partial\left(\frac{yL}{Gr^{\frac{1}{4}}}\right)} \left(\frac{v}{L}Gr^{\frac{1}{2}}u \right) \right) + g\beta T(T'_w - T'_\infty) - \sigma_0 \frac{\beta_0^2 \frac{v}{L}Gr^{\frac{1}{2}}u}{\rho}$$

$$\Rightarrow \frac{\partial u}{\partial t} + u \frac{\partial u}{\partial x} + v \frac{\partial u}{\partial y} = \left[e^{-\lambda t} \frac{\partial^2 u}{\partial y^2} - \lambda e^{-\lambda t} \frac{\partial T}{\partial y} \frac{\partial u}{\partial y} \right] + T - \sigma_0 \frac{\beta_0^2 L^2 Gr^{-\frac{1}{2}}}{\rho v} u$$

$$\Rightarrow \frac{\partial u}{\partial t} + u \frac{\partial u}{\partial x} + v \frac{\partial u}{\partial y} = \left[e^{-\lambda t} \frac{\partial^2 u}{\partial y^2} - \lambda e^{-\lambda t} \frac{\partial T}{\partial y} \frac{\partial u}{\partial y} \right] + T - Mu \tag{9}$$

Again the energy equation (3) can be reduced by the above similarity transformation (5) and (7), we have

$$\Rightarrow \frac{\partial\{T'_\infty + T(T'_w - T'_\infty)\}}{\partial\left(\frac{tL^2}{vGr^{\frac{1}{2}}}\right)} + \frac{vu}{L}Gr^{\frac{1}{2}} \frac{\partial\{T'_\infty + T(T'_w - T'_\infty)\}}{\partial(xL)} + \frac{vv}{L}Gr^{\frac{1}{4}} \frac{\partial\{T'_\infty + T(T'_w - T'_\infty)\}}{\partial\left(\frac{yL}{Gr^{\frac{1}{4}}}\right)}$$

$$= \frac{1}{\rho C_p} \frac{\partial}{\partial\left(\frac{yL}{Gr^{\frac{1}{4}}}\right)} \left(k \frac{\partial\{T'_\infty + T(T'_w - T'_\infty)\}}{\partial\left(\frac{yL}{Gr^{\frac{1}{4}}}\right)} \right) + \frac{\{T'_\infty + T(T'_w - T'_\infty)\} \beta u v Gr^{\frac{1}{2}}}{\rho C_p L} \frac{\partial P}{\partial(xL)}$$

$$\Rightarrow \frac{\partial T}{\partial t} + u \frac{\partial T}{\partial x} + v \frac{\partial T}{\partial y} = \frac{1}{P_r} \left[\gamma \left(\frac{\partial T}{\partial y} \right)^2 \right] + \frac{1}{P_r} \left[(1 + \gamma T) \frac{\partial^2 T}{\partial y^2} \right] - \left\{ \left(T + \frac{T'_\infty}{(T'_w - T'_\infty)} \right) \right\} G_e \mu \quad (10)$$

The Corresponding initial condition and boundary condition in dimensionless forms are as follows

$$\begin{aligned} t \leq 0: u = 0, v = 0, T = 0 \text{ for all } y, \quad t > 0: u = 0, v = 0, T = 1 \text{ at } y = 0 \\ u = 0, T = 0 \text{ at } x = 0, \quad u \rightarrow 0, T \rightarrow 0 \text{ at } y \rightarrow \infty \end{aligned} \quad (11)$$

Equations (8) to (10) with the boundary condition (11) describe the free convective unsteady laminar boundary layer flow with variable viscosity and thermal conductivity

along an isothermal semi- infinite vertical plate. Where, $M = \sigma_0 \frac{\beta_0^2 L^2 Gr^{\frac{1}{2}}}{\mu}$ is the magnetic parameter, $Pr = \mu_0 C_p / k_0$ is the Prandtl's number and $Ge = \frac{g \beta L}{C_p}$ is the pressure work parameter.

The local shear stress in the plate is defined by

$$\tau_{\bar{x}} = \left(\mu \frac{\partial \bar{u}}{\partial \bar{y}} \right)_{\bar{y}=0} \quad (12)$$

By introducing the non-dimensional quantities given in equations (5)-(6) in (12), we get non-dimensional form of local skin friction and it is given by

$$\begin{aligned} \tau_{\bar{x}} = \left(\mu \frac{\partial \bar{u}}{\partial \bar{y}} \right)_{\bar{y}=0} \Rightarrow \frac{L^2}{\nu \mu_0} \tau_{(xL)} = Gr^{\frac{3}{4}} e^{-\lambda} \left[\frac{\partial u}{\partial y} \right]_{y=0} \\ \therefore \bar{\tau}_x = Gr^{\frac{3}{4}} e^{-\lambda} \left[\frac{\partial u}{\partial y} \right]_{y=0} \end{aligned} \quad (13)$$

The integration of equation (13) from $x=0$ to $x=1$ gives the average skin friction and it is given by

$$\bar{\tau} = e^{-\lambda} Gr^{\frac{3}{4}} \int_0^1 \left(\frac{\partial u}{\partial y} \right)_{y=0} dx \quad (14)$$

The local Nusselt number is defined by

$$Nu_{\bar{x}} = \frac{-L \left(k \frac{\partial T'}{\partial \bar{y}} \right)_{\bar{y}=0}}{k_0 (T'_w - T'_\infty)}$$

$$\Rightarrow \bar{Nu}_x = -(1 + \gamma) \left(\frac{\partial T}{\partial y} \right)_{y=0}$$

$$\therefore \bar{Nu}_x = -(1 + \gamma) \left(\frac{\partial T}{\partial y} \right)_{y=0} \tag{15}$$

The integration of equation (15) from $x=0$ to $x=1$ gives the average skin friction and it is given by

$$\therefore Nu_x = -(1 + \gamma) \int_0^1 \left(\frac{\partial T}{\partial y} \right)_{y=0} dx \tag{16}$$

NUMERICAL TECHNIQUES

Under the initial and boundary conditions in Equation (11) the two-dimensional, non-linear, unsteady, and coupled partial differential Equations (8)-(10) are solved using an implicit Crank-Nicolson type finite difference scheme that is fast convergent and unconditionally stable. The finite difference equation corresponding to Equations (8) to (10) are given by

$$\frac{\left[u_{i,j}^{k+1} - u_{i-1,j}^{k+1} + u_{i,j}^k - u_{i-1,j}^k + u_{i,j-1}^{k+1} - u_{i-1,j-1}^{k+1} + u_{i,j-1}^k - u_{i-1,j-1}^k \right]}{4\Delta x} + \frac{\left[v_{i,j}^{k+1} - v_{i,j-1}^{k+1} + v_{i,j}^k - v_{i,j-1}^k \right]}{2\Delta y} = 0$$

$$\tag{17}$$

$$\frac{\left[u_{i,j}^{k+1} - u_{i,j}^{k+1} \right]}{2\Delta t} + u_{i,j}^k \frac{\left[u_{i,j}^{k+1} - u_{i-1,j}^{k+1} + u_{i,j}^k - u_{i-1,j}^k \right]}{2\Delta x}$$

$$v_{i,j}^k \frac{\left[u_{i,j+1}^{k+1} - u_{i,j-1}^{k+1} + u_{i,j+1}^k - u_{i,j-1}^k \right]}{4\Delta y} = \frac{1}{2} \left[T_{i,j}^{k+1} + T_{i,j}^k \right]$$

$$\begin{aligned}
 & +e^{-\lambda} \left[\frac{T_{i,j}^{k+1} + T_{i,j}^k}{2} \right] \frac{[u_{i,j-1}^{k+1} - 2u_{i,j}^{k+1} + u_{i,j+1}^k + u_{i,j-1}^k - 2u_{i,j}^k + u_{i,j+1}^k]}{2(\Delta y)^2} \\
 & + \\
 & -\lambda e^{-\lambda} \left[\frac{T_{i,j}^{k+1} + T_{i,j}^k}{2} \right] \frac{[T_{i,j+1}^{k+1} - T_{i,j-1}^{k+1} + T_{i,j+1}^k - T_{i,j-1}^k]}{4\Delta y} \frac{[u_{i,j+1}^{k+1} - u_{i,j-1}^{k+1} + u_{i,j+1}^k - u_{i,j-1}^k]}{4\Delta y} \\
 & - \frac{M}{2} [u_{i,j}^{k+1} + u_{i,j}^k]
 \end{aligned} \tag{18}$$

$$\begin{aligned}
 & \left[\frac{T_{i,j}^{k+1} - T_{i,j}^k}{2\Delta t} \right] + u_{i,j}^k \frac{[T_{i,j}^{k+1} - T_{i-1,j}^{k+1} + T_{i,j}^k - T_{i-1,j}^k]}{2\Delta x} + v_{i,j}^k \frac{[T_{i,j-1}^{k+1} - T_{i,j-1}^{k+1} + T_{i,j+1}^k - T_{i,j-1}^k]}{4\Delta y} \\
 & = \frac{1 + \gamma T_{i,j}^k}{Pr} \frac{[T_{i,j-1}^{k+1} - 2T_{i,j}^{k+1} + T_{i,j+1}^k + T_{i,j-1}^k - 2T_{i,j}^k + T_{i,j+1}^k]}{2(\Delta y)^2} + \\
 & \frac{\gamma}{Pr} \left[\frac{[T_{i,j+1}^{k+1} - T_{i,j-1}^{k+1} + T_{i,j+1}^k - T_{i,j-1}^k]}{4\Delta y} \right]^2 - \left[\frac{1}{2} \{T_{i,j}^{k+1} + T_{i,j}^k\} + \frac{T'_\infty}{T'_w - T'_\infty} \right] \frac{1}{2} (u_{i,j}^{k+1} + u_{i,j}^k) Ge
 \end{aligned} \tag{19}$$

The region of integration is considered as a rectangle with sides $x_{\max}(= 1)$ and $y_{\max}(=10)$, where y_{\max} Corresponds to $y = \infty$, which lies very well outside the momentum and energy boundary layers. The maximum of y was chosen as 6 after some preliminary investigations so that the last two of the boundary conditions (11) are satisfied. Here, the subscript i -designates the grid point along the u -direction, j -along the v -direction and the superscript k along the t -direction. During any one time step, the coefficients $u_{i,j}^k$ and $v_{i,j}^k$ appearing in the difference equations are treated as constants. The values of u , v and T are known at all grid points at $t = 0$, from the initial conditions. The computations of u , v and T at time level $(k + 1)$ using the values at previous time level (fe) are carried out as follows: the finite difference Eq. (18) at every internal nodal point on a particular i -level constitute a tridiagonal system of equations. Such a system of equations is solved by Thomas algorithm as described in Carnahan *et al.* [19]. Thus, the values of T are found at every nodal point for a particular i at $(k + 1)^{\text{th}}$ time level. Using the values of T at $(k + 1)^{\text{th}}$ time level in the Eq. (13), the values of u at $(k + 1)^{\text{th}}$ time level are found in a similar manner. Thus, the values of T and u are known on a particular i -level. Finally, the values of v are calculated explicitly using the Eq. (12) at every nodal point on a particular i -level at $(k + 1)^{\text{th}}$ time level. This process is repeated for various i -

levels. Thus the values of T , u and v are known, at all grid points in the rectangular region at $(k + 1)^{\text{th}}$ time level.

After considering with few sets of mesh sizes, they have been fixed at the level $\Delta x = 0.05$, $\Delta y = 0.25$, and the time step $\Delta t = 0.01$. In this case, spatial mesh size is reduced by 50% in one-direction then in both directions, and the results are compared. It is observed that, when mesh size is reduced by 50% in x -direction and y -direction the results differ in fourth decimal place. Hence the above mentioned sizes have been considered as appropriate mesh size for calculations. Computations are carried out until the steady-state is reached. The steady-state solution is assumed to have been reached, when the absolute difference between the values of u , as well as temperature T at two consecutive time steps are less than 10^{-5} at all grid points. The local truncation error is $O(\Delta t^2 + \Delta F^2 + \Delta Ax)$ and it tends to zero as Δt , Δx and Δy tend to zero, which shows that the scheme is compatible. Also the Crank-Nicolson type of implicit finite difference scheme is proved to be unconditionally stable for a natural convective flow in which there is always a non-negative value of velocity u and a non-positive value of v . Thus, compatibility and stability ensures the implicit finite difference scheme is convergent.

RESULTS AND DISCUSSION

The direct microscopic exchange of kinetic energy of particles across the boundary between two structures is known as heat conduction, also known as diffusion. Water is a strong heat transfer fluid because of its high thermal ability and low viscosity. Oil has a higher liquid temperature than water, so it's been a popular option for avoiding the problem of high pressure. Heat is transferred between the Earth's surface and the atmosphere by conduction, radiation, and convection. Heat is transferred by convection when a heated fluid, such as air or water, is forced to travel away from the source of heat, bringing energy with it. Convection happens as hot air expands, becomes less dense, and rises over a hot surface. Since liquid metals have a low Prandtl's number, heat transfer by molecular thermal conduction is important not only in the near-wall layer, but also in the flow center, even in a fully developed turbulent flow. The following ranges for λ , γ and Pr are considered in the present study are:

For air: $-0.7 \leq \lambda \leq 0, 0 \leq \gamma \leq 6, Pr = 0.733$

For water: $0 \leq \lambda \leq 0.6, 0 \leq \gamma \leq 0.12, 2 \leq Pr \leq 7.00$

In order to check the accuracy of our computed values, we compare our results with the curves computed by G.palani.Kwang-Yong Kim and Elbashbeshy & Ibrahim for various values of γ and fixed values of $\lambda = 0.40, M = 0.00, Ge = 0.00$ for air ($Pr = 0.733$). These are plotted in Figs. 2(a), 2(b). Our results agree very well with those of G.palani.Kwang-Yong Kim and Elbashbeshy & Ibrahim at the steady state.

The body force has not had enough time to produce an effective motion in the fluid during the initial phase following step changes in the wall temperature. As a result, for small time t , the velocity components u and v are both negligible. Pure heat conduction dominates heat transfer during this initial transient regime, resulting in constant viscosity and thermal conductivity. Equation (10) reduces to

$$\frac{\partial T}{\partial t} = \frac{1}{Pr} \frac{\partial^2 T}{\partial y^2}$$

Thus, for a given Prandtl's number, magnetic parameter, and normal distance from the wall, the temperature profile is only a function of time and normal distance from the wall for short periods. Setting $Pr = 1$, the solutions of Eq. (15) subject to the initial and boundary conditions given in local Nusselt's number are

$$T = \operatorname{erfc}\left(\frac{y}{2\sqrt{t}}\right) \quad (20)$$

For different viscosity, thermal conductivity, magnetic variation parameters, and Prandtl's numbers, Figures 3.2(a), 3.2(b), 3.3(a), 3.3(b), 3.4(a), 3.4(b), 3.5(a), 3.5(b), 3.6(a), 3.6(b), 3.7(a), 3.7(b), 3.8(a), 3.8(b), 3.9(a), 3.9(b), 3.10(a), 3.10(b), 3.11(a), 3.11(b) show the variation of velocity and temperature at their transient, temporal limit, and steady state against the co-ordinate y at the leading edge of the plate, viz., $x = 1.0$. For all time t , the fluid velocity increases until it reaches its maximum value very close to the wall (i.e., $0 \leq y \leq 2$), and then monotonically decreases to zero as y becomes larger. It's also worth noting that the velocity and temperature rise with time t , reach a temporal limit, and then settle into a steady state.

The variance of transient velocity and temperature profiles with area A for fixed values of $\gamma = 0.20, M = 0.30, Ge = 0.50$ in air ($Pr = 0.733$) is shown in Figures 3(a) and 3(b).

The fluid's velocity increases over time until it reaches a temporal limit, after which it gradually decreases until it reaches the ultimate steady state. It is observed that as the viscosity variance parameter is increased, the time taken to reach the steady state decreases slightly. The velocity u at any vertical plane near the plate increases as x increases (the viscosity of air decreases), as shown in Fig. 3(a). At a certain distance from the wall, however, the opposite pattern is observed. The temperature of the fluid decreases as λ increases, as shown in Fig. 3(b) (the viscosity of air decreases).

The numerical values of the variation of transient velocity and temperature profiles with γ for a fixed value of $\lambda = -0.60$, $Ge = 0.30$, $M = 0.40$ in air ($Pr = 0.733$) with the variation of thermal conductivity parameter γ are shown graphically in Figs. 4(a) and 4(b). For fixed values of λ , M , Ge , and Prandtl's number, it can be shown that the velocity and temperature distribution in the fluid increases as γ increases (thermal conductivity of air increases). It's also worth noting that as γ increases, the magnitude of the velocity and temperature increases significantly, implying that the volume flow rate increases as γ increases. Even during the initial transient phase, the effect of thermal conductivity variation on velocity and temperature is more important. With increasing the thermal conductivity parameter γ , the time to hit the temporal limit and steady state decreases.

Figures 5(a) and 5(b) show the numerical values of variance velocity and temperatures determined from Eqs. (13) and (14) for different values of λ for fixed values of $M = 0.50$, $\gamma = -0.30$, $Ge = 0.40$ in water ($Pr = 3.00$). It is obvious that as the viscosity variance parameter λ is increased, the time taken to reach the temporal maximum and steady state decreases. Since the viscosity of water decreases with an increase in the viscosity variation parameter λ , as seen in Eq. 5, an increase in the viscosity variation parameter λ increases the velocity of the flow near the wall (6). For higher values of λ , the maximum velocity also gets very close to the wall. This qualitative effect occurs because the fluid with variable viscosity ($\lambda > 0$) is able to pass more easily in a region close to the heated surface due to the lower viscosity of the fluid with $\lambda > 0$ compared to the fluid with constant viscosity. As a consequence, the velocity and thermal boundary layers become thinner. The velocity of the fluid particle increases only in the

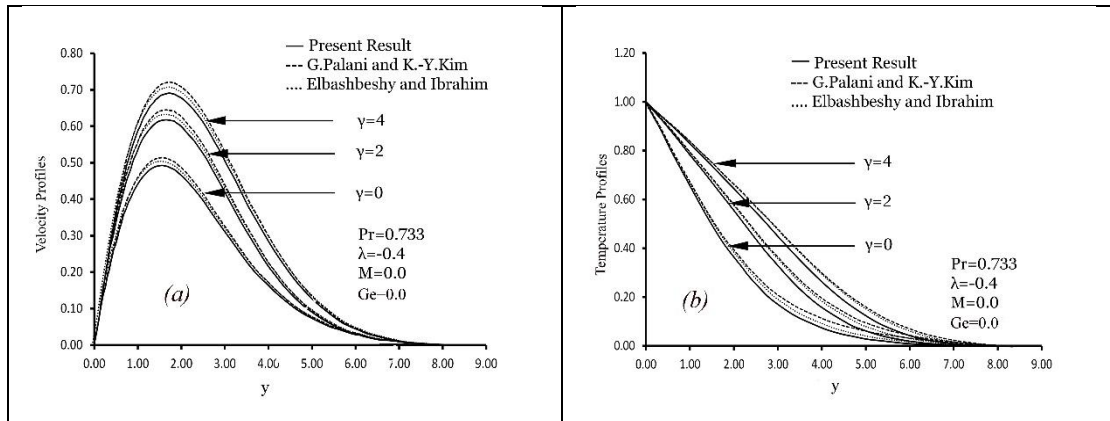
area $0 \leq y \leq 2$ as λ increases (the viscosity of water decreases). The temperature profiles decrease with increasing λ , as shown in Fig.5 (b). This is due to the fact that an increase in λ results in an increase in peak velocity. The first effect increases the velocity of the fluid particle due to a decrease in viscosity, while the second effect reduces the velocity of the fluid particle due to a decrease in temperature near the plate, where T is high. As a result, the first force will be dominant, and the velocity u will increase as λ increases. When the temperature T is low far away from the plate, however, the second effect takes over, and the velocity decreases as λ increases. We can see from the discussion that ignoring the difference of fluid viscosity and thermal conductivity can result in a significant mistake.

The variance of velocity and temperature for different values of γ for fixed values of $\lambda=0.40$, $M=0.50$, $Ge=0.50$ in water ($Pr=3.00$) is shown in Figures 6(a) and 6(b).

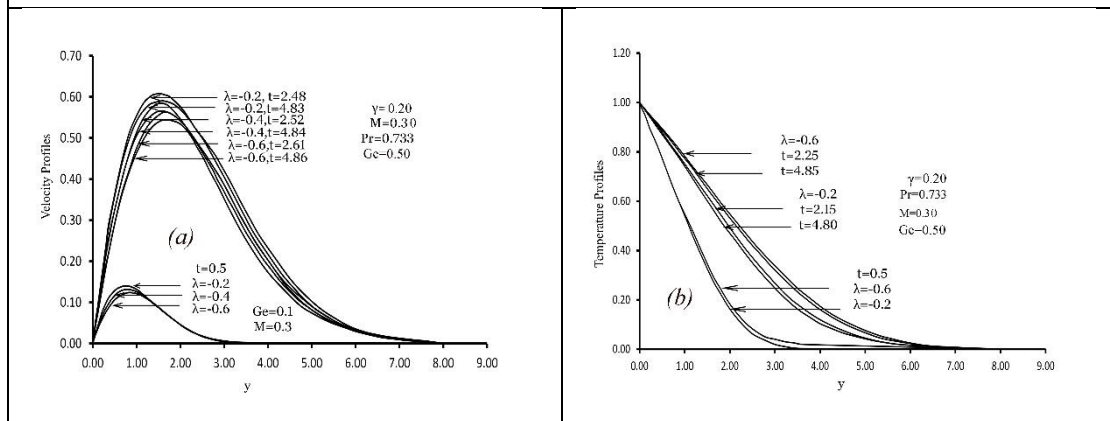
It has been found that as the value of γ increases, the time it takes to reach the steady state decreases. It's also worth noting that as the value of γ rises, so does the temperature distribution of the fluid. Figures 7(a) and 7(b) show the velocity and temperature profiles for various values of the pressure work parameter Ge for specific values of Pr , λ , γ , and M under steady state conditions. As can be seen in Fig.7 (a), an increase in the pressure work parameter Ge is correlated with a significant increase in velocity profiles, but near the plate's surface, the velocity increases and becomes maximum, then decreases and asymptotically reaches zero. However, for certain values of the pressure work parameter Ge , Fig.7(b) shows the distribution of temperature profiles against y .

The temperature distribution clearly increases with rising values of the pressure work parameter Ge , with the limit being at the plate wall's edge. Figures 8(a) and 8(b) display the variance of transient velocity and temperature with Prandtl's numbers for fixed values of $\lambda=0.30$, $\gamma=0.40$, and $M=0.40$. With increasing Prandtl's number of the fluid, it is observed that the time taken to reach the temporal limit and steady state increases. We can see from the numerical results that the velocity profile decreases as Prandtl's number increases. Since a greater Prandtl's number value indicates that the thermal diffusion from the wall is not prevailing, while the velocity diffusion spreads further from the wall, thinner temperature profiles result. In Figs. 9(a) and 9(b), the numerical values of variance of velocity and temperature profiles with M are

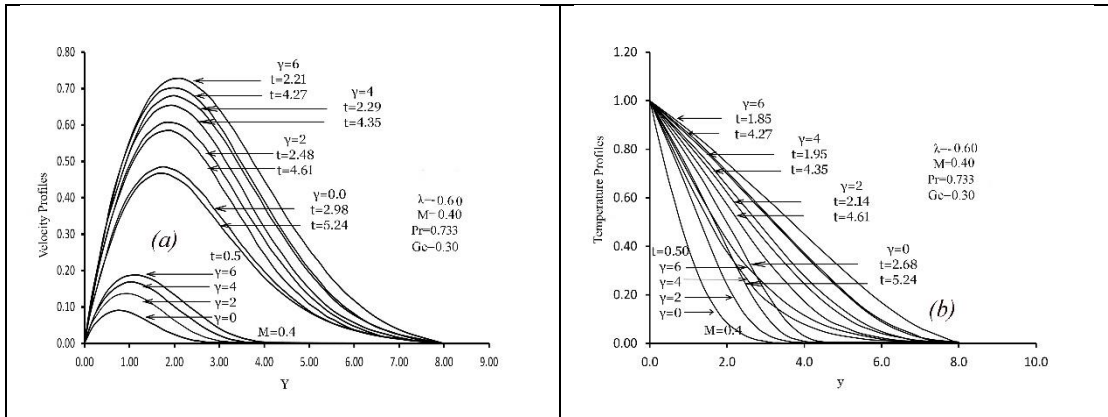
graphically shown for fixed values of $\lambda = 0.50$, $\gamma = -0.10$ for air ($Pr = 0.733$). It can be seen from these graphs that the time it takes to enter the steady state increases as the magnetic parameter M decreases. It's also worth noting that as M gets closer to the vertical plate, the velocity rises. As the magnetic parameter M decreases, the temperature of the fluid decreases.



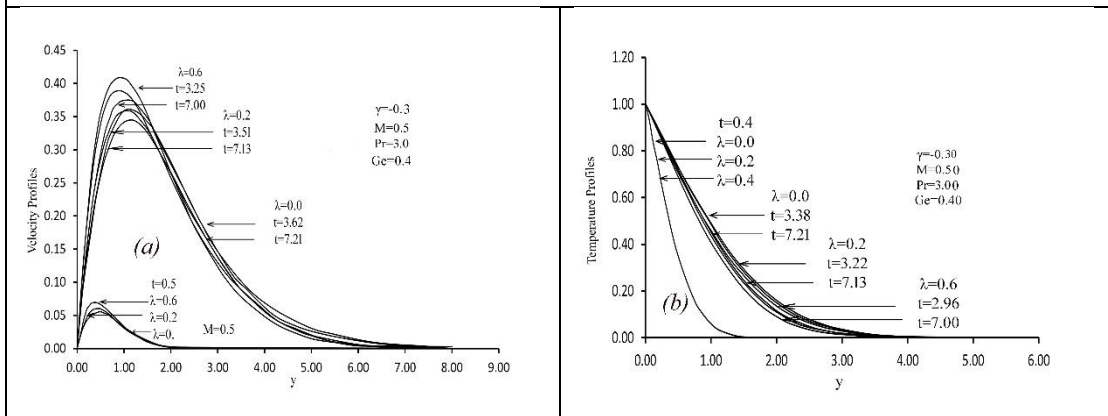
Figures 2(a) and 2(b): Variation of dimensionless velocity profiles and temperature profiles against dimensionless y for different values of variable thermal conductivity parameter γ with $Pr = 0.733$, $\lambda = 0.40$, $Ge = 0.0$ and $M = 0.0$.



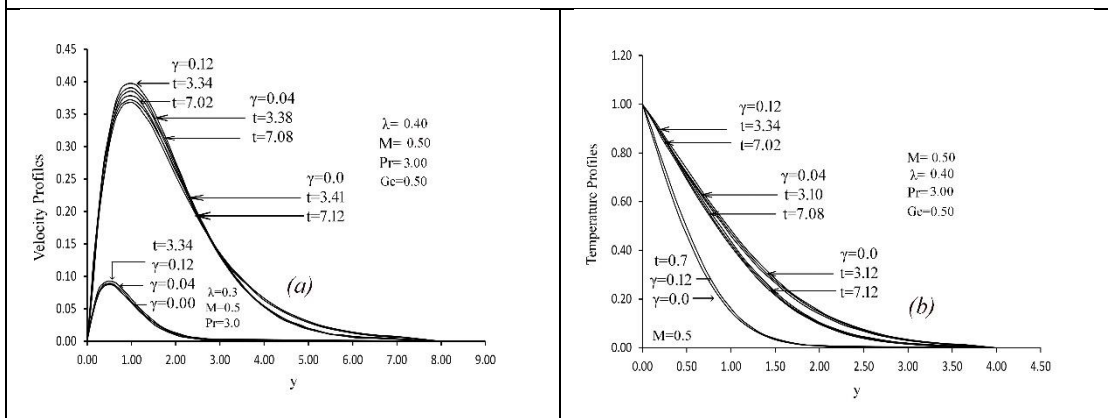
Figures 3(a) and 3(b): Variation of dimensionless velocity profiles and temperature profiles against dimensionless y for different values of variable viscosity parameter λ and steady state condition with $Pr = 0.733$, $\gamma = 0.20$, $Ge = 0.30$ and $M = 0.50$.



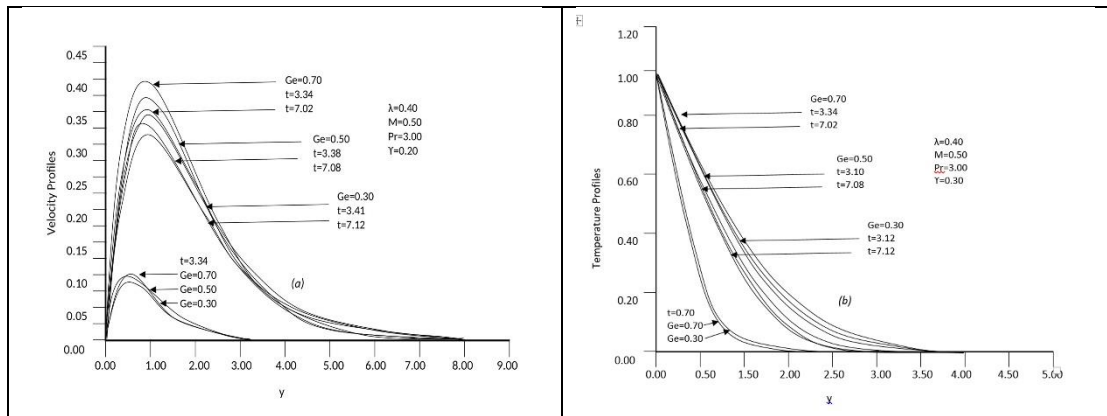
Figures 4(a) and 4(b): Variation of dimensionless velocity profiles and temperature profiles against dimensionless y for different values of variable thermal conductivity parameter γ and steady state condition with $Pr = 0.733$, $\lambda = 0.60$, $Ge = 0.30$ and $M = 0.40$.



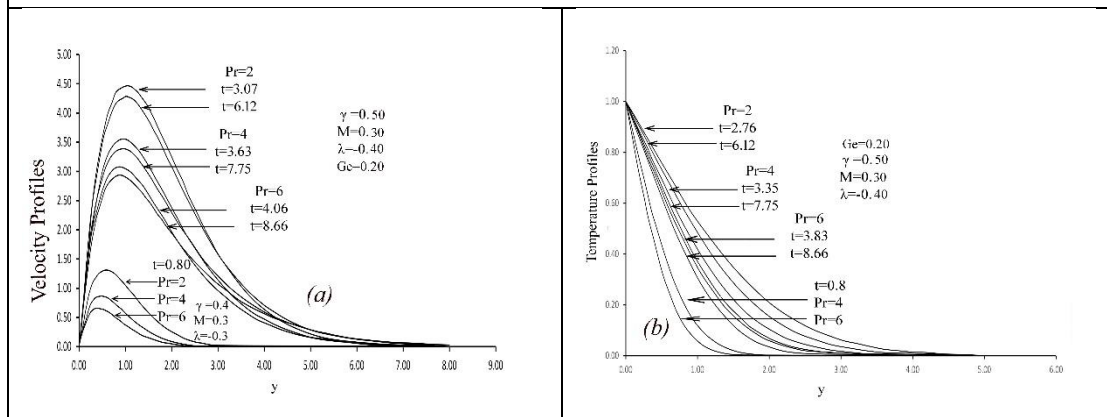
Figures 5(a) and 5(b): Variation of dimensionless velocity profiles and temperature profiles against dimensionless y for different values of variable viscosity parameter λ and steady state condition with fixed values $Pr = 3.00$, $\gamma = 0.30$, $Ge = 0.40$ and $M = 0.50$.



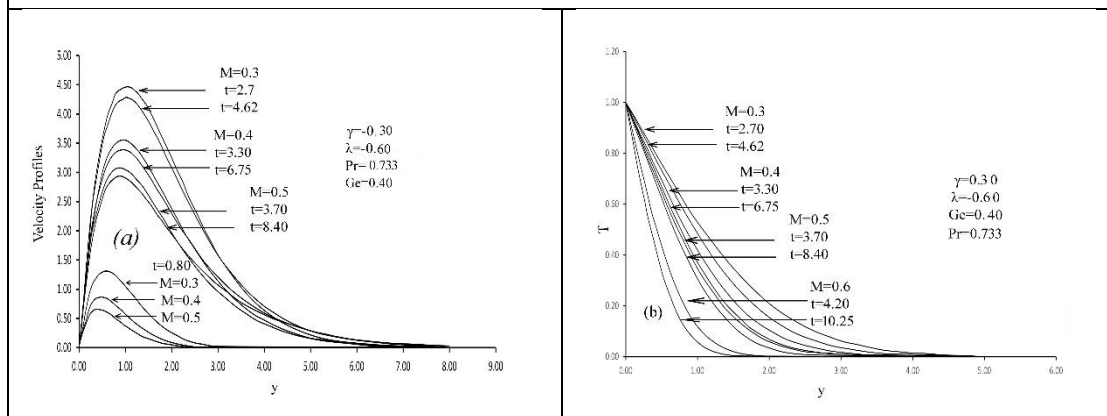
Figures 6(a) and 6(b): Variation of dimensionless velocity profiles and temperature profiles against dimensionless y for different values of variable thermal conductivity parameter γ and steady state condition with fixed values $Pr = 3.00$, $\lambda = 0.40$, $Ge = 0.50$ and $M = 0.50$.



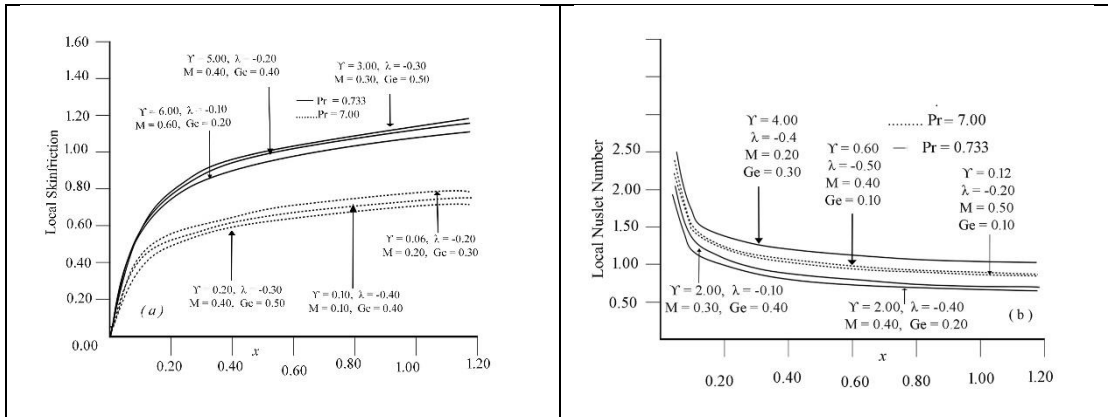
Figures 7(a) and 7(b): Variation of dimensionless velocity profiles and temperature profiles against dimensionless y for different values pressure work parameter Ge and steady state condition with $\lambda = 0.30$, $\gamma = 0.40$ and $M = 0.40$.



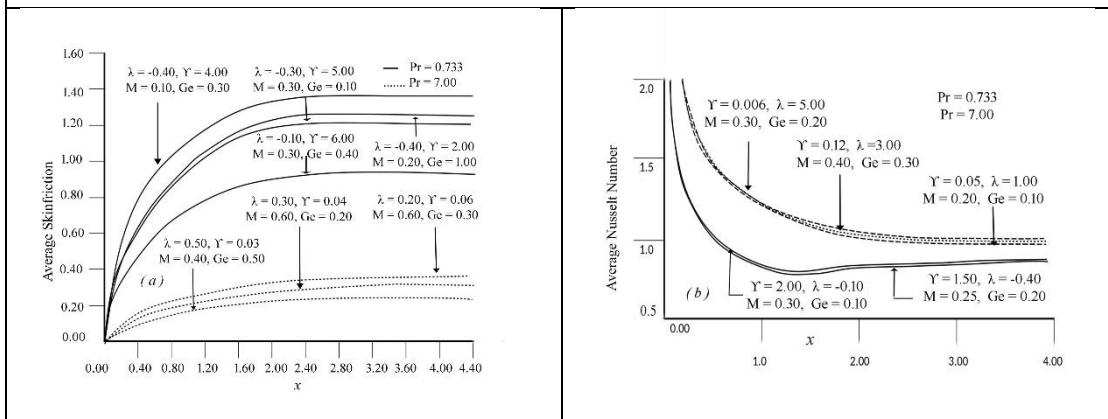
Figures 8(a) and 8(b): Variation of dimensionless velocity profiles and temperature profiles against dimensionless y for different values of Prandtl's number Pr and steady state condition with fixed values $\lambda = 0.40$, $\gamma = 0.50$, $Ge = 0.20$ and $M = 0.30$.



Figures 9(a) and 9(b): Variation of dimensionless velocity profiles and temperature profiles against dimensionless y for different values of magnetic parameter M and steady state condition with fixed values $\lambda = 0.60$, $\gamma = 0.30$, $Ge = 0.40$ and $Pr = 0.733$.



Figures 10(a) and 10(b): Variation of dimensionless local skin friction and local Nusselt number against dimensionless distance x for different values of M , Ge , λ , γ and Pr at steady state condition.



Figures 11(a) and 11(b): Variation of dimensionless average skin friction and average Nusselt number against dimensionless distance x for different values of M , Ge , λ , γ and Pr at steady state condition.

Eqs. (12), (14), (15), and (16) include the evaluation of derivatives using a five-point approximation formula, followed by the evaluation of integrals using the Newton-Cotes closed integration formula. Eq. (13) is used to calculate the local skin-friction values, which are then plotted in Fig. 10(a) as a function of the axial coordinate λ for air and water, as well as selected values of the variation parameters λ , γ , M , and Ge . As λ rises, so does the local skin friction. It is observed that as the value of viscous variation parameter λ increases, local skin friction decreases. It's also worth noting that as the value of thermal conductivity parameter γ rises, so does the local wall shear stress.

Local skin friction is found to decrease as the value of Prandtl's number rises. For different values of viscosity and thermal conductivity parameters for air and water, average values of skin friction are determined numerically from Eq. (14) and

graphically shown in Fig. 11(a). It increases over time and reaches a stable state after a period of time. With increasing values of viscous parameter λ , pressure work parameter Ge , and magnetic parameter M , average skin friction decreases. It's also worth noting that as the value of thermal conductivity parameter γ increases, the average wall shear stress increases as well. Average skin friction is observed to decrease as the value of Prandtl's number increases. For different values of variance parameters, Fig.10 (b) indicates a dimensionless steady state local heat transfer rate for air and water. The rate of local heat transfer is found to increase as the viscosity, thermal conductivity, and magnetic parameters increase. The rate of local heat transfer increases as Pr increases. Since a larger Pr results in a thinner thermal boundary layer, a larger wall temperature gradient, and thus a higher heat transfer rate, this pattern is anticipated. The effects of variance parameters and Pr on the average Nusselt number are shown in Fig. 11(b). Since increasing the Prandtl number speeds up the spatial decay of the temperature in the flow region, resulting in an increase in the rate of heat transfer, but on the opposite side for the magnetic parameter, increasing the Prandtl number leads to an increase in the average heat transfer rate. It's also worth noting that as λ , γ , Ge , and M decrease, the average Nusselt number decreases.

CONCLUSION

The effect of variable viscosity and thermal conductivity on magneto-hydrodynamics laminar natural convection boundary-layer vertical plate with stress work and constant surface temperature is studied in this paper. The thermal conductivity is assumed to be a linear function of temperature and the fluid viscosity is assumed to be an exponential function of temperature. An implicit Crank-Nicolson style finite difference scheme is used to solve the dimensionless governing equations. Graphically, a distinction is made between the current numerical findings and previously published works. The arrangement between the two parties is deemed to be excellent.

According to the findings of this study:

- (i) The dimensionless fluid velocity increases as the viscosity parameter λ increases and the fluid temperature decreases. Higher velocity is observed

in a region near the wall when the viscosity variance parameter λ is significant, resulting in a higher Nusselt number and lower skin friction.

- (ii) The fluid velocity, fluid temperature, the dimensionless wall velocity gradient, and the dimensionless rate of heat transfer from the plate to the fluid all increase as the thermal conductivity parameter γ increases.
- (iii) With higher values of the pressure work parameter, the time to achieve the temporal limit and steady state decreases. Ge causes the velocity and temperature distributions to widen.
- (iv) It's worth noting that ignoring viscosity and thermal conductivity variations can result in significant errors. As a result, we conclude that the effects of variable viscosity and thermal conductivity must be considered in order to predict more accurate outcomes.
- (v) The local skin friction coefficient, the local Nusselt number, and the velocity distribution over the entire boundary layer decrease with the impact of magnetic parameter M , but the temperature distribution increases with the steady state condition.

REFERENCES

- [1] Alam MM, Alim MA, Chowdhury MMK. Effect of pressure stress work and viscous dissipation in natural convection flow along a vertical flat plate with heat conduction, *Journal of Naval Architecture and Marine Engineering*, 2006;3(2): 69-76.
- [2] Alim M A, Alam MM, Al-Mamun Abdullah, Joule heating effect on the coupling of conduction with magneto-hydrodynamic free convection flow from a vertical flat plate, *Nonlinear Analysis: Modeling and Control*. 2007;.12(3): 307-316.
- [3] Rahman M.M, Mamun A A, Azim MA, Alim MA, Effects of temperature dependent thermal conductivity on MHD free convection flow along a vertical flat plate with heat conduction, *Nonlinear Analysis: Modeling and Control*. 2008;13(4): 513-524.
- [4] Alim MA, Alam MM, Al-Mamun Abdullah Hossain Belal, The combined effect of viscous dissipation & Joule heating on the coupling of conduction & free convection along a vertical flat plate. *International Communications in Heat and Mass Transfer*. 2008; 35(3): 338-346.
- [5] Safiqul Islam A.KM, Alim M A, Sarker MMA, Khodadad Khan AFM, Effects of temperature dependent thermal conductivity on natural convection flow along a vertical flat plate with heat generation, *Journal of Naval Architecture and Marine Engineering*. 2012;9(2): 113-122.
- [6] Kabir KH, Alim MA, Andallah LS, Effects of viscous dissipation on MHD natural convection flow along a vertical wavy surface. *Journal of Theoretical and Applied Physics. an Springer Open Journal*. 2013; 7(31) 1-8.
- [7] Hossain MA, Viscous and Joule heating effects on MHD free convection flow with variable plate temperature. 1992; 35 (2): .3485-3487.
- [8] Soundalgekar, VM, Ganesan, P, Finite difference analysis of transient free convection on an isothermal flat plate. *Reg. J. Energy Heat Mass Transf*. 1981; 3; 219-224.

- [9] Elbashbeshy, EMA, Ibrahim, FN, Steady free convection flow with variable viscosity and thermal diffusivity along a vertical plate. *J. Phys. D Appl. Phys.* 1993;26(12): 237-2143.
- [10] Kafoussius, NG, Rees, DAS, Numerical study of the combined free and forced convective laminar boundary layer flow past a vertical isothermal flat plate with temperature dependent viscosity. *Acta Mech.* 1998; 127(11): 39-50.
- [11] Elbashbeshy, EMA, Dimian, MF, Effect of radiation on the flow and heat transfer over a wedge with variable viscosity. *Appl. Math. Comput.* 2002; 132: 445-454.
- [12] Anwar Hossain, Khalil M, K., Kambi MV, The effect of radiation on free convection flow of fluid with variable viscosity from a porous vertical plate. *Int. J. Therm. Sci.* 2001;40: 115-124.
- [13] Seddeek, MA, Effect of variable viscosity on a MHD free convection flow past a semi-infinite flat plate with an aligned magnetic field in the case of unsteady flow. *Int. J. Heat Mass Transf.* 2002; 45: 931-935.
- [14] Carnahan B, Luther HA, Wilkes JO, *Applied Numerical Methods.* Wiley, New York.1969.
- [15] Siattery, J.C *Momentum, Energy and Mass Transfer in Continua.* McGraw Hill, New York. 1972.
- [16] Ockendon, H, Ockendon, JR, Variable-viscosity flows in heated and cooled channels. *J. Fluid Mech.* 1977; 83(1): 177-190.
- [17] Seddeek, MA., Abdelmeguid, MS, Effects of radiation and thermal diffusivity on heat transfer over a stretching surface with variable heat flux. *Phys. Lett. A* . 2006; 348(3-6): 172-179.
- [18] Palani, G, and Kim, KY, Numerical study on vertical plate with variable viscosity and thermal conductivity. Springer-Verlag. 2009; 80: 711-725.
- [19] Carnahan, B, Luther, HA, Wilkes, JO, *Applied Numerical Methods.* Wiley, New York. 1969.